Carnegie Observatories Astrophysics Series, Vol. 3:
Clusters of Galaxies: Probes of Cosmological Structure and Galaxy Evolution, 2004
ed. J. S. Mulchaey, A. Dressler, and A. Oemler (Pasadena; Carnegie Observatories:
http://www.ociw.edu/ociw/symposia/series/symposium3/proceedings.html)

The Dark Matter Distribution in Galaxy Cluster Cores

M. W. BAUTZ and J. S. ARABADJIS
Massachusetts Institute of Technology Center for Space Research, Cambridge, MA, USA

Abstract

Galaxy cluster mass distributions offer an important test of the cold dark matter picture of structure formation, and may even contain clues about the nature of dark matter. X-ray imaging spectroscopy of relaxed systems can map cluster dark matter distributions, but are usually complicated by the presence of central cool components in the intracluster medium. Here we describe a statistically correct approach to distinguishing amongst simple alternative models of the cool component, and apply it to one cluster. We also present mass profiles and central density slopes for five clusters derived from *Chandra* data, and illustrate how assumptions about the cool component affect the resulting mass profiles. For four of these objects, we find that the central density profile ($r < 200\mathrm{h}_{50}^{-1}$ kpc) $\rho(r) \sim r^{\alpha}$ with $-2 < \alpha < -1$, for either of two models of the central cool component. These results are consistent with standard CDM predictions.

1.1 Introduction

The cold dark matter (CDM) paradigm successfully describes many aspects of the formation of large-scale structure in the universe (Lahav *et al.* 2001; Peacock *et al.* 2001; Navarro, Frenk & White 1997; Moore *et al.* 1999b). Galaxy-scale dark matter halos, however, exhibit several apparent inconsistencies with CDM, for example: the number of Milky Way satellites appears to be at least an order of magnitude lower than CDM predictions (Kauffman, White, & Guideroni 1993; Moore *et al.* 1999a; Klypin *et al.* 1999), and dark matter halos in dwarf and low surface brightness galaxies are much less cuspy than in CDM simulations (Burkert 1995; McGaugh & de Blok 1998; Moore *et al.* 1999b). Some reports (Tyson, Kochanski & Dell'Antonio 1998; Smail *et al.* 2000) even suggest that CDM fails on galaxy cluster scales for some clusters, but the latter are controversial (Broadhurst *et al.* 2000; Shapiro & Iliev 2000).

Proposed modifications of CDM include self-interacting dark matter (Spergel & Steinhardt 2000; Firmani *et al.* 2000), warm dark matter (Hogan & Dalcanton 2000), annihilating dark matter (Kaplinghat, Knox & Turner 2000), scalar field dark matter (Hu & Peebles 2000; Goodman 2000), and mirror matter (Mohapatra, Nussinov & Teplitz 2002), each of which is invoked to soften the core density profile. Many of these modifications will soften the core profile of galaxy clusters as well, although other astrophysical processes such as the adiabatic contraction of core baryons (Hennawi & Ostriker 2002) may ameliorate this effect. Baryons, however, introduce a host of complications to CDM simulations (Frenk 2002).

In order better to discriminate among CDM, its modifications, and other astrophysical influences, we are mapping the dark matter profiles of a sample of galaxy cluster cores. We use imaging spectroscopy from the *Chandra X-ray Observatory* (our own observations – Arabadjis, Bautz & Garmire 2002 – and those in the *Chandra* archive) to deproject the radial profile of the intracluster medium (ICM) density and temperature for each cluster. In order to extract a dark matter profile from spatially resolved X-ray spectroscopy one usually assumes that the galaxy cluster is spherically symmetric and in hydrostatic equilibrium, and so for the most part we have restricted our sample to clusters for which, to judge from their *Chandra* X-ray images, these assumptions appear to be valid. As noted by Allen (1998), clusters in hydrostatic equilibrium often contain "cooling flows," or cool components in their cores, and these components must be properly modelled if reliable inferences about cluster mass are to be drawn. If the model of the ICM contains only a single emitting component (at temperature T and density ρ) at each radius, the inferred temperature profile will tend to dip significantly toward the center of a cluster with a cool component. If, however, gas in the the core contains a second (cooler) component which is cospatial and isobaric with the first, then a hot ICM component coexists with the cool component in the core. The latter case tends to produce a larger central mass (see Figures 1.1) and steeper density profile than the former.

In this contribution, we first discuss the proper method for distinguishing between these two simple models, and then present results for mass profiles for a number of clusters.

1.2 One Temperature or Two?

1.2.1 Approach

Our problem is to choose between a simple model M^{s}, representing a single-component core ICM, and a complex model M^{c}, representing two-phase gas. In order to test for the presence of a second emission component we adopt a simplified geometry containing only two spherical shells (inner = 1, outer = 2). In both models (M^{s} and M^{c}), shell 2 contains a (hot) thermal plasma at temperature T_{2h} and density ρ_{2h}. Model M^{s} contains only one emission component in shell 1, characterized by a temperature T_{1h} and a density ρ_{1h}, whereas model M^{c} contains a hot and a cool emission component in shell 1, described by T_{1h}, ρ_{1h}, T_{1c}, and ρ_{1c}. The X-ray emission from each component is modelled spectroscopically using the MEKAL model (see, e.g., Liehdal, Osterheld & Goldstein 1995) as implemented in the XSPEC software package (Arnaud 1996). The best-fit parameter values of each model are calculated using a χ^2 minimization routine. Hereafter we will refer to the simple and complex model parameters using vectors θ^{s} and θ^{c}, respectively; i.e., $\theta^{\mathsf{s}} = (T_{1h}, \rho_{1h}, T_{2h}, \rho_{2h})$ and $\theta^{\mathsf{c}} = (T_{1h}, \rho_{1h}, T_{1c}, \rho_{1c}, T_{2h}, \rho_{2h})$.

It might seem straightforward to apply a conventional test such as the likelihood ratio test or the F-test (Bevington 1969; Cash 1979) to choose between the two models. However, since θ^{s} lies on a boundary of θ^{c} (with $\rho_{1c} = 0$), these tests cannot be employed (Protassov *et al.* 2002). Instead, we construct an *empirical* F-distribution using Markov Chain Monte Carlo (MCMC) sampling, and gauge the significance of the complex model from the location of the F value of the data within that distribution (Protassov *et al.* 2002).

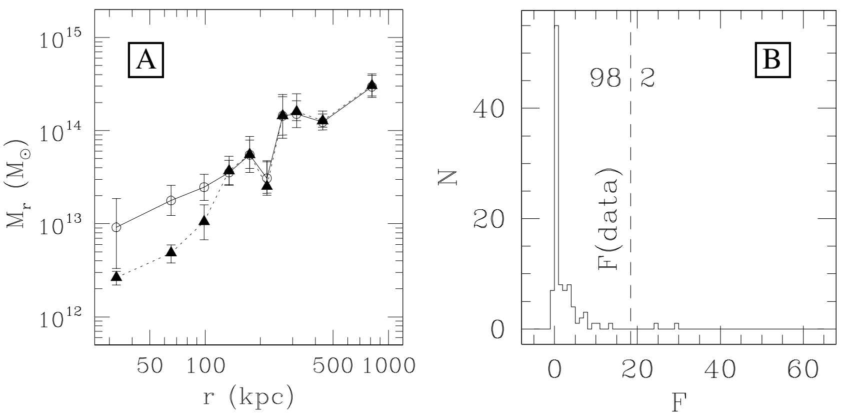

Fig. 1.1. [A] One- and two-temperature mass profiles (dotted/triangles and solid/circles, respectively) of EMSS 1358+6245; [B] empirical F-distribution for models $\mathsf{M^s}$ and $\mathsf{M^c}$ of EMSS 1358+6245.

1.2.2 An Empirical "*F*-distribution"

We briefly summarize our computation of an empirical "F-distribution" here; details will be presented elsewhere (Arabadjis & Bautz, in preparation). Starting with the best-fit parameters θ_0 of model $\mathsf{M^s}$, we sample the 4D parameter space in its vicinity using MCMC sampling. This is done by running a Tcl script within XSPEC which calculates the probability distribution function P of a trial perturbation θ_1 about θ_0 given the observed data. The trial point is chosen using the trial distribution function $q(\theta_0, \theta_1)$. The choice of q is arbitrary; we restrict ourselves to functions which are symmetric in parameter space transitions, i.e. $q(\theta_i, \theta_j) = q(\theta_j, \theta_i)$. This new parameter set is accepted if $P(\theta_1)/P(\theta_0)$ exceeds a random number on [0,1]. If not, the trial point is rejected and new one is selected. The sequence of accepted θ_i is a Markov Chain whose stationary distribution follows $P(\theta)$ (Lewis & Bridle 2002). We repeat this procedure until we have 100 values of θ for model $\mathsf{M^s}$.

For each of the parameter sets in the sample we simulate an X-ray spectrum, taking proper account of the instrument response and photon statistics. We then model each of the simulated data sets using both $\mathsf{M^s}$ and $\mathsf{M^c}$, and tabulate the F-value of each data set:

$$F = \frac{\chi^2(\theta^s) - \chi^2(\theta^c)}{\chi^2(\theta^s)/\nu(\mathsf{M^s})} \tag{1.1}$$

where $\nu(\mathsf{M^s})$ is the number of degrees of freedom of the simple model. (In practice, the normalization can be ignored.) The F-distribution for the cooling flow cluster EMSS 1358+6245 is shown in panel B of Figure 1.1. The F-value of the original *Chandra* data set is indicated with a dashed line.

1.2.3 An Example: MS1358+6245

Of the 100 MCMC simulations that were run, only two resulted in an F-value which exceeded that of the data – that is, if $\mathsf{M^s}$ were the correct description, an F-value as large as that observed would occur with a probability of only 2% – meaning that the model with a separate, co-spatial cool component is preferred. The result is that a model with a steeper density profile and a larger central mass is favored. If this trend obtains for most cooling flow clusters, it may rule out several of the CDM modifications.

1.3 Mass Profiles and Core Slopes

We have yet to apply the foregoing analysis to discriminate between 1- and 2-temperature models to all clusters in our sample. Instead, here we merely illustrate, in Figure 1.2, the sensitivity of the derived mass profile and inferred density slope in the cluster core to the assumed state of the intracluster medium for five reasonably relaxed clusters. These results have been obtained using the deprojection methods described in Arabadjis, Bautz & Garmire (2002). The left panel of Figure 1.2 shows that, generally, the inferred mass is larger, the encircled mass profile marginally flatter, and, in consequence, the density somewhat steeper in the 2-temperature model.

The right panel of Figure 1.2 shows the logarithmic density slope parameter α (here defined so that the central density $\rho(r) \sim r^{\alpha}$) inferred from the mass profile for each cluster. (We plot α against redshift merely as a convenient means of display.) The indices shown were obtained by fitting the mass profile within $r < 200$ h_{50}^{-1} kpc, which is typically about one-tenth the virial radius inferred from the best-fit NFW profiles for these objects. We note that the core slopes are generally consistent with, or slight steeper than, the standard CDM results ($-1.5 < \alpha < -1.0$; Navarro, Frenk & White 1997; Moore *et al.* 1999b).

1.4 Summary

We have illustrated a rigorous and quantitative procedure for distinguishing between emission models of cool components in clusters. We have presented mass profiles derived from *Chandra* X-ray images for five clusters, using both 1- and 2-temperature models for the central X-ray emission. In almost all cases we find that the slope of the total central mass density is consistent with, or slightly steeper than, standard CDM predictions.

References

Allen, S. W. 1998, MNRAS, 296, 392

Arabadjis, J. S., Bautz, M. W., & Garmire, G. P. 2002, ApJ, 572, 66

Arnaud, K. A. 1996, in Astronomical Data Analysis Software and Systems V, George H. Jacoby & Jeannette Barnes, eds., ASP Conf. Ser., 101, 17

Bevington, P. R. 1969, Data Reduction and Error Analysis for the Physical Sciences (New York: McGraw-Hill)

Broadhurst, T., Huang, X., Frye, B., & Ellis, R. 2000, ApJ, 534, 15

Burkert, A. 1995, ApJ, 447, L25

Cash, W. 1979, ApJ, 228, 939

Firmani, C., D'Onghia, E., Avila-Reese, V., Chincarini, G., & Hernández, X. 2000, MNRAS315L29

Frenk, C. S. 2002, Phi. Trans. Roy. Soc., 300, 1277

Goodman, J. 2000, New Astron., 5, 103

Hennawi, J. F., & Ostriker, J. P. 2002, ApJ, 572, 41

Hogan, C. J. & Dalcanton, J. J. 2000, Phys. Rev. D, 62, 063511

Hu, W., & Peebles, P. J. E. 2000, ApJ, 528, 61

Kaplinghat, M., Knox, L., & Turner, M. S. 2000, Phys. Rev. Lett., 85, 3335

Kauffmann, G., White, S. D. M., & Guiderdoni, B. 1993, MNRAS264201

Klypin, A. A., Kravtsov, A. V., Valenzuela, O., & Prada, F. 1999, ApJ, k522, 82

Lahav, O., *et al.*2001, MNRAS, 333, 961

Lewis, A., & Bridle, S. 2002, Phys. Rev. D, 66, 103511

Liedahl, D. A., Osterheld, A. L., & Goldstein, W. H. 1995, ApJL, 438, L115

McGaugh, S. S., & de Blok, W. J. G. 1998, ApJ, 499, 41

Mohapatra, R. N., Nussinov, S., & Teplitz, V. L. 2002, Phys. Rev. D, 66, 063002

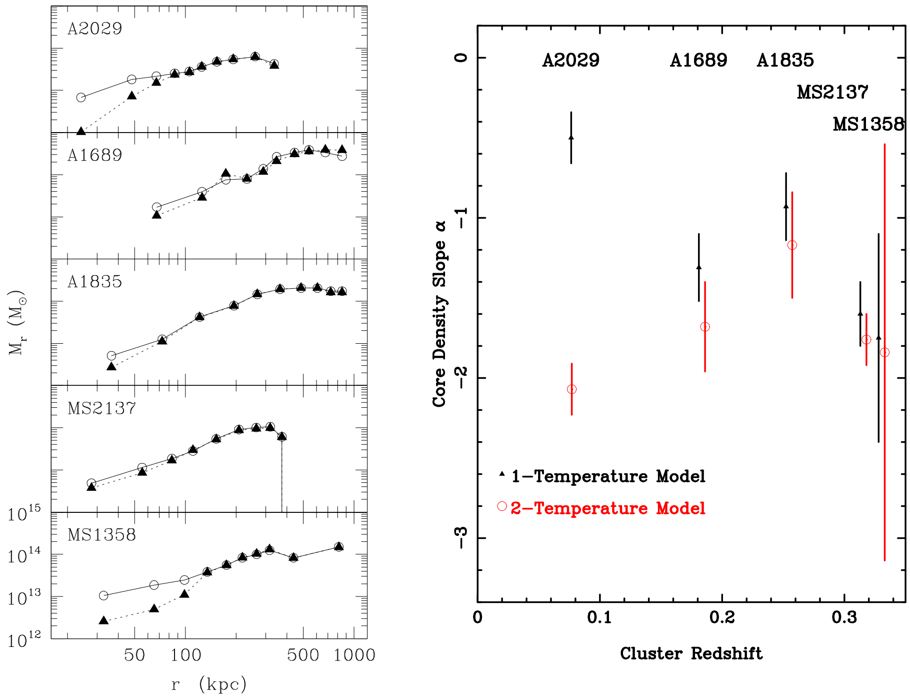

Fig. 1.2. *Left:* *Chandra* mass profiles, assuming 1-temperature and 2-temperature central emission models, (dotted/triangles and solid/circles, respectively) for 5 clusters. Masses and radii for $H_0 = 0, \Omega_m = 1$. *Right:* Core density power-law index α (for $\rho(r) \sim r^{\alpha}$) determined within $r < 200$ h_{50}^{-1} kpc for the same clusters, using 1- and 2-temperature models (open circles & filled triangles, respectively.) The error bars show 90%-confidence intervals for α.

Moore, B., Ghigna, S., Governato, F., Lake, G., Quinn, T., Stadel, J., & Tozzi, P. 1999a, ApJL, 524, L19
Moore, B., Quinn, T., Governato, F., Stadel, J., & Lake, G. 1999, MNRAS3101147
Navarro, J. F., Frenk, C. S., & White, S. D. M. 1997, ApJ, 490, 493
Peacock, J. A., *et al.*2001, Nature, 410, 169
Protassov, R., van Dyk, D. A., Connors, A., Kashyap, V. K.w & Siemiginowska, A. 2002, ApJ, 571, 545
Shapiro, P. R., & Iliev, I. T. 2000, ApJL, 542, L1
Smail, I., Ellis, R., Ritchett, M. J., & Edge, A. C. 1995, MNRAS273277
Spergel, D. N., & Steinhardt, P. J. 2000, Phys. Rev. Lett., 84, 17
Tyson, J. A., Kochanski, G. P., & Dell'Antonio, I. P. 1998, ApJ, 498, L107